Reconstruction of the Holocene hydro-ecological and environmental change of the Nile Delta: insights from organic geochemical records in MZ-1 sediment core

Fan Zhang[a,b,c], Jianfang Hu[b], Xinxin Li[a,d*], Yanna Wang[e*], Chengpeng Sun[a], Xin Zhao[a], Xiaoshuang Zhao[e], Feng Jiang[e], Yan Liu[e], Alaa Salem[f], A. M Abu Shama[f], Zhongyuan Chen[e]

a) Shenzhen Key Laboratory of Marine Archaea Geo-Omics, Department of Ocean Science and Engineering, Southern University of Science and Technology, Shenzhen 518055, Guangdong, China

b) State Key Laboratory of Organic Geochemistry, Guangzhou Institute of Geochemistry, Chinese Academy of Sciences (GIGCAS), Guangzhou, 510640, China

c) School of Earth and Space Sciences, University of Science and Technology of China, Hefei 230026, China

d) Southern Marine Science and Engineering Guangdong Laboratory (Guangzhou), Guangzhou, 511458, Guangdong, China

e) State Key Laboratory for Estuarine and Coastal Research, East China Normal University, Shanghai 200062, China

f) Kafrelsheikh University, Faculty of Science, Kafrelsheikh, Egypt

[*]**Corresponding authors: lixinxin@sustech.edu.cn; ynwang@sklec.ecnu.edu.cn**

Abstract

The Holocene hydro-ecological and environmental change of the Nile Delta remains a knowledge gap. The study aimed to approach this objective by using multi-proxies of organic carbon (OC) in a well-dated MZ-1 core in Manzala lagoon off the Nile Delta. The data defined five distinctive stages at decadal-centennial scale. Stage I (ca. 8.2-7.7 ka) was characterized by remarkedly high reconstructed pH and low mean annual air temperature (the 8.2-ka cold event). The obviously low TOC and C/N, but higher short-chain n-alkanes indicated more marine OC deposition. This was followed by highly fluctuated organic geochemical proxies at Stage (ca. 7.7-5.8 ka) indicating episodic but significant terrestrial OC input delivered by Nile floods during the African Humid Period (AHP). Subsequent increase in short- and medium-chain n-alkanes suggested macrophytes prevailing in the lagoon during Stage (ca. 5.8-5.4 ka) with cooling-drying climate transitioned from the AHP. Stage (ca. 5.4-1.2 ka) witnessed decreased short-chain n-alkanes of marine origin and increased long-chain n-alkanes of terrestrial origin when the Nile climate entered into the mega-trend of aridification. Abnormal pulses of terrestrial OC with high TOC likely reflected the modified landscape due to early human occupation around the area. The highly fluctuated charcoal fluxes since ca. 6 ka implied such

clearing-firing-aided land exploitation activity. The lagoon eco-setting was further affected by intensified anthropogenic-OC input after the latest millennium. Our study highlighted the land-ocean interactions on modulating the paleo-lagoonal ecology of the Nile Delta, which should be incorporated into healthy management in the Nile Delta.

Key words: African Humid Period; organic carbon; tetra either lipids; land-ocean interaction; decadal-centennial scale; human activities

Highlights:

1. Terrestrial OC delivered by immense episodic Nile floods significantly impacted the eco-setting of the Nile lagoon during 7.7-5.8 ka;

2. Reconstructed MAAT and pH suggested a climate transition from later AHP to mega-aridification with enhanced brackish ecology;

3. Buried OC documented freshwater-marine-human intervened ecological condition of the Nile Delta in the Holocene.

1. Introduction

The Holocene witnessed significant climatic changes and land-sea interactions with their immense impact on geo-ecological soundness in densely-populated delta-coast, especially in the climatically sensitive arid Nile Delta (Kuper & Kröpelin, 2006; Blanchet et al., 2014; Clarke et al., 2016). The paleo-ecological condition of the Nile Delta had been imprinted by the African Humid Period (AHP) (generally ca. 11.0-5.5 ka) and consequent mega-trend of aridification of north Africa due to southward-withdrawing of the Intertropical Convergence Zone (ITCZ) (deMenocal et al., 2000; Shanahan et al., 2015; Tierney et al., 2017). The Nile Delta was to form at ca. 7.0 ka when sea-level rise began to stabilize. The newly-formed coast then was gradually occupied by the early settlers, who created the flourishing Egyptian civilization. Therefore, to trace the history of hydro-ecological-human intervened coastal environment change can shed light not only on the process-response of geo-mechanism, but also on future development (Chandan & Peltier, 2020; Pausata et al., 2020).

The Nile River drains a basin of 3.35 million km^2 across the North Africa. Spatially, it covers a wide range of latitudes (Figure 1A) and integrates catchment-wide hydroclimate records (Weldeab et al., 2014; Castañeda et al., 2016). As is a worldwide focus, the Nile Delta (Figure 1B) serves as a breadbasket for the early agricultural development, which can be traced back to 7000 years ago (Stanley & Warne, 1993a; Zhao et al., 2020). The delta is mainly beneficial from its hydrological fluctuations in context of high-frequency of floods from the Nile catchment (Butzer, 1979; Said, 1981). Flooded aggradation had built the delta-plain a higher topography of ca. 15 m above the mean sea level (amsl) at Cairo (delta apex) vs 1-2 m (amsl) on coast, across a distance of ca. 200 km (Figure 1B). The delta sediment has kept rich information of basin-wide hydroclimate

fluctuations, marine signals, and the early human activities in the Holocene time (Rachmayani et al., 2015). It is thus an ideal study site for reconstructing the paleo-hydro-ecological-human complex.

The bulk OC and lipid biomarker proxies of core sediment have been widely used to reconstruct the paleo-environmental conditions at various scales (Meyers, 1994; Lamb et al., 2006; Schouten et al., 2013; De Jonge et al., 2014). The stable isotope of ^{13}C, total organic carbon (TOC) and carbon to nitrogen (C/N) ratios were applied to track OC sources (eg. Li et al., 2013) with related environment changes, such as sea-level rise, flow oscillations, and human impacts (Li et al., 2011, 2013). The n-alkanes are effective in recovering the proportion of paleo-vegetation since different plants and microorganisms are characterized by the unique chain length and preference of carbon numbers (Bush & McInerney, 2013). The glycerol dialkyl glycerol tetraethers (GDGTs) are membrane-spanning lipids of bacteria and archaea, and their structures change in response to specific environmental parameters such as mean annual air temperature (MAAT) and pH (Weijers et al., 2007), therefore to be able to reflect distinctive environmental settings (Schouten et al., 2013).

In order to reveal the environmental changes during the Holocene, the present study used bulk OC and lipid biomarkers in sediment core MZ-1 on Manzala lagoon-coast to reconstruct the hydro-ecological-human forcing and their role in modifying coastal setting, the sole geo-ecological gate for Egyptian connecting the Mediterranean Sea. The study objectives are: 1) to reconstruct process-response of high-resolution hydro-climatic fluctuations (freshwater and seawater) in the delta coast, specifically during the AHP and the mega-aridification time; 2) to identify varied sources of OC of the lagoon-coast and related environmental implications in the Holocene; and 3) to trace for, in light of OC proxies, the contribution of early farming activities to modified eco-setting, where the earliest human occupation occurred.

2. Study area, materials and methods

2.1 Study area and coring

A 19.5-m long sediment core (MZ-1) was taken using rotary machine on Manzala Lagoon coast in northeastern Nile Delta (31°05 18.76 N, 32°08 14.55 E) (Figure 1B). The core sediment was received continuously by drilling corer with 9 cm in diameter and 1.0 m long. Core samples were well kept in wooden box and transported back to the laboratory for analysis. The sediment core was split into two halves, one for sampling and the other for archiving. Sedimentary logging was applied to core sediments, including lithology, sediment color, water content, and biogenic occurrences. Core sediment was photographed throughout. Sampling at a 10-cm interval proceeded, totaling 142 samples for this study. The top 1.5 m was the contemporary agricultural soil, and thus not considered for any sampling test in this study.

2.2 Radiocarbon dating

In total, 12 samples consisting of charcoal and shells were selected for radiocarbon dating (Table 1) using Accelerator Mass Spectrometry (AMS) at Beta Analytic, Florida, USA. The "rBacon" package in R software was applied to calibrate the ^{14}C dates to the calendar years, used for the constructing age-depth model (Blaauw & Christen, 2011). Charcoal samples were calibrated with the IntCal20 curve (Reimer et al., 2020), while shell samples were calibrated using the Marine20 calibration curve (Heaton et al., 2020). All ages are calibrated years before present (cal. yrs. BP), expressed as ka in this study.

2.3 Grain size and charcoal analysis

Approximately 1-g sample was dried at 40 °C for 24 h. Then 10% HCl was added to eliminate carbonate, and 10% H_2O_2 was added to remove organic matter. Finally $(NaPO_3)_6$ was added to disperse the sediment. The grain size analysis was conducted using a Beckman Coulter Laser Diffraction Particle Size Analyzer (Model: LS13320; Measurement range: 0.04–2000 m).

A total of 44 samples were selected for micro-charcoal analysis and 2-6 g dried sediment each was firstly treated with HCl solution (15%) for 24 hours to remove carbonates. Lycopodium clavatum tablet was added to each sample before acid processing. The treated samples were oxidized and desilicated by HF solution (> 40%) for 24 hours. The treated solution after each step was rinsed by Milli-Q water for 4-7 times to remove extra acid. The refractory charcoal particles in the residue were isolated through filtration by Normesh (Φ 10 µm) in ultrasonic cleaner. Both charcoal and Lycopodium clavatum were counted under microscope at a magnification of 400×.

At least 300 charcoal particles over 50 µm length were counted for each sample. The charcoal abundance of each sample was calculated with Lycopodium clavatum counting and expressed as grains/g/sample. The charcoal particles were classified into two groups based on particle size: 50-100 µm (micro-charcoal) and 100 µm (macro-charcoal). The ratio of length (major axis) to width (minor axis) of macro-charcoal (L/W) of each sample was presented. Charcoal flux is used in present study.

2.4 Bulk organic carbon analysis

Freeze-dried and homogenized sediment (ca.1g) was treated with 4 mol/L HCl and left for 24 hours. After washed with deionized water until pH=7 and oven dried at 60℃, TOC, TN, ^{13}C and ^{15}N were analyzed by Elemental Analyzer and Stable-isotope mass spectrometer (Sercon HS20-22). The laboratory standards are Acetanilide (^{13}C=-26.85‰, ^{15}N=-4.21‰) and IAEA-600 (^{13}C=-22.77‰, ^{15}N=1‰). The average standard deviations were <0.5% for TOC, <0.3% for TN, <0.2‰ for ^{13}C and ^{15}N.

2.5 Lipid analysis

Total lipids were extracted according to De Jonge et al. (2014). Briefly, freeze-dried and homogenized samples were spiked with internal standards (C36 cholestane and C46 $GDGT_{46}$). After extraction by Accelerated Solvent Extractor (ASE 150, Dionex), the total lipid extract (TLE) was saponified. The neutral components on an active silica gel colomn were extracted by n-hexane. Apolar (n-alkanes involved) and polar (GDGTs involved) fractions were subsequently fractionated from the neutral components on an active silica gel column by elution with hexane (apolar fraction) and DCM: MeOH (3:1 v/v, polar fraction), respectively. The n-alkanes were analyzed by gas chromatography (Agilent Technologies 7890). The quantification was based on their integrated peak areas compared with those of the internal standard C36 cholestane. The short-chain n-alkanes (C15–C20), medium-chain n-alkanes (C21–C25), and long-chain n-alkanes (C27-C33) with clear odd-over-even carbon preference were used as biomarkers for microorganisms, submerged- or floating-leaved aquatic plants, and terrestrial plants, respectively (Bush & McInerney, 2013). The index of Paq was calculated as the ratio of C23+C25 to C23+C25+C29+C31 to indicate the proportion of aquatic plant contribution (Ficken et al., 2000).

The polar components were dissolved in DCM and filtered through 0.45 m polytetrafluoroethylene filters. After concentrated by nitrogen, the GDGTs were dissolved in hex: ethyl acetate (84:16, v:v) for High-performance liquid chromatography (Agilent 1200 series)/atmospheric pressure chemical ionization-mass spectrometry (Thermo TSQ Vantage) (HPLC/APCI-MS) analysis. The injection volume was 20 µL and the flow rate was set to 0.2 mL/min. The absolute concentration and relative abundance of different GDGT components were obtained from integrated peak areas of mass chromatograms relative to C_{46} GDGT.

The branched and isoprenoid tetraether (BIT) index (Hopmans et al., 2004) reflects the relative abundance of major brGDGTs over crenarchaeol, and implies the proportion of terrigenous OC inputs:

$$BIT = \frac{Ia + IIa + IIa' + IIIa + IIIa'}{Ia + IIa + IIa' + IIIa + IIIa' + crenarchaeol} \quad (1)$$

The methylation of branched tetraethers index (MBT) is related to MAAT (De Jonge et al., 2014) and the cyclization of branched tetraethers index (CBT) correlates solely with soil pH (Weijers et al., 2007; De Jonge et al., 2014):

$$\text{MBT} = \frac{Ia + Ib + Ic}{Ia + Ib + Ic + a + b + c + a} \quad (2)$$

$$\text{MAAT} = -8.57 + 31.45 * \text{MBT} \quad (3)$$

$$\text{CBT} = \log 10 \frac{Ic + a' + b' + c' + a' + b' + c'}{Ia + a + a} \quad (4)$$

$$\text{pH} = 7.15 + 1.59 * \text{CBT} \quad (5)$$

All the roman letters corresponding to specific GDGTs were following the defi-

nition by Schouten et al. (2013).

2.6 Statistical analysis

To quantify the contribution of various OC sources to the sedimentary OC pool, a three end-member (soil, marine OC, macrophyte) mixing model of Bayesian approach was applied using "Simmr" package in R software. The endmember values of ^{13}C and N/C for "Simmr" were: -20 ± 5‰ and 0.069 ± 0.013 for soil (Abebe et al., 2020), -20 ± 2‰ and 0.15 ± 0.05 for marine OC (Fry & Sherr, 1989; Hedges & Oades, 1997), and -24 ± 2‰ and 0.063 ±0.021 for macrophyte (Khedr & El-Demerdash, 1997; Lamb et al., 2006). The principal component analysis (PCA) of all the parameters analyzed was also employed using the R software.

3. Results

3.1 Holocene strata and charcoal distribution

The basal core sediment (19.5-17.7m) is composed of massive yellow medium- to coarse-sand (>125 µm) with modeled ^{14}C age > 36.0 ka (Figure 2A). This coarser sediment was regarded usually as the fluvial sand deposited during the Late Pleistocene when sea level was lower, and the study area was subaerially exposed (Stanley & Warne, 1993b). Core sediment of 17.7-16.4 m (ca. >12-10 ka) consists of light yellowish fine- to medium-sand and silt with Fe-Mn lenses and nodules (Figure 2A, B), showing the pre-Holocene sediment hiatus before Holocene marine invasion into the Manzala coast.

The sediment section of 16.4-4.0 m (ca. 9.0-5.0 ka) was made up of a chunk of darkish gray muds, with silty laminae (Figure 2A, B) and enriched in shells (whole and fragments). This sediment section was usually referred as typical lagoonal deposits. The 4.0-1.5 m (ca 5.0-0.5 ka) was made up of light yellowish sand and grayish mud (<4 µm) without shells (Figure 2B).

Dating framework allows to work out sedimentation rates of MZ-1. There occurred the remarkably high sedimentation rate of ca. 1.0 cm/year between 9.0-5.0 ka, which is followed by an extremely low sedimentation rate of 0.02-0.06 cm/year after ca. 5.0 ka (Figure 2C). Regardless varied sedimentation rates, core MZ-1 showed continuous sedimentation during the Holocene, ensuring to approach the study goal of this environmental reconstruction.

The charcoal flux (50 m) of 44 samples varied from 2.2×10^2 to 2.6 $\times10^5$ grains/cm^2/yr with an average value of 2.9 $\times10^4$ grains/cm^2/yr. Apparently, there were two phases in temporal variation (Figure 2D). In the section below core depth 7.4 m (before ca. 5.7 ka), the flux kept stable in general (Figure 2D): ca.1.8×10^4 grains/cm^2/yr for macro-charcoal and 1.2×10^5 grains/cm^2/yr for micro-charcoal. Since then (above core depth 7.4 m), both micro-and macro-charcoal fluxes were highly fluctuated in distribution upwards in core sediment,

with a few peaks between 4.9-5.6 ka (Figure 2D). The charcoal flux descended since ca. 4.9 ka (4.2 m) and reached its minimum of 3.2 grains/cm^2/yr around 1000 years ago (Figure 2D). The L/W ratio also witnessed the two phases similar to charcoal flux, but slightly rose with fluctuations in the second phase (Figure 2D).

3.2 Bulk organic carbon

The TOC content ranged from 0.02% to 1.72% (0.69±0.34%) (Figure 3A). TN varied with TOC (Figure 3B) with a positive correlation (r^2=0.82, $p<0.05$), suggesting that the N was mainly in organic forms. The ^{15}N was from -8.14‰ to 5.91‰ (1.1±2.5‰) (Figure 3C). The ^{13}C values varied between -27.00‰ and -17.52‰ (-20.05±1.39‰) (Figure 3D). Five Stages can be defined on the basis of temporal variations of bulk OC.

Stage (16.4-15.9 m): ca. 8.2 to 7.7 ka

It was characterized by the lowest TOC (0.11±0.02%, Figure 3A), TN (0.02±0.002%, Figure 3B), variable ^{15}N (0.82±3.25‰, Figure 3C) and ^{13}C values (-21.26±1.17‰, Figure 3D), and low C/N ratios (6.7±0.5, Figure 3D), suggesting features of marine-derived OC.

Stage (15.9-8.0 m): 7.7 to ca. 5.8 ka

There was a prominent transition between Stage and Stage , in which TOC, ^{13}C and C/N values showed an abrupt increase, from 0.14% to 0.81%, -21.3 to -19.1‰ and 7.1 to 13.6, respectively (Figure 3A, D). The TN and ^{15}N were stable during this stage (Figure 3B, C). Terrestrially-derived OC significantly influenced the buried OC. As a result, at least eight peaks with higher C/N and lower ^{13}C were observed (Figure 3D), indicating a major interference of OC sourced from terrestrial environment. For example, the average C/N and ^{13}C of the eight peaks were 22.5±2.1, and -21.17±0.62‰, which were significantly higher than that of the average values of this stage (16.3±2.0 and -19.66±0.39‰) (Figure 3D).

Stage (8.0-5.7 m): ca. 5.8-ca. 5.4 ka

Stage featured differently from Stage . At least three peaks with lower C/N and higher ^{13}C than the average values at this stage were observed (Figure 3D), Such excursions were caused by reduced contribution from terrestrial OC due to the post-AHP drying condition. As a result, the marine-OC relatively increased in the OC pool with lower TOC (0.57±0.25) (Figure 3A).

Stage (5.7-1.9 m): ca. 5.4-ca. 1.2 ka

The bulk OC proxies in Stage were characterized by increased TOC, TN, ^{15}N and C/N and decreased ^{13}C (Figure 3A-D), indicating episodic high terrestrial OC input. The extremely low sedimentation rate (0.02-0.06 cm/year) was observed during this stage (Figure 2C).

Stage (1.9-1.5 m): ca. 1.2-ca. 0.74 ka

Almost all OC proxies had abrupt changes in Stage V (Figure 3). TOC, TN and ^{15}N increased remarkably by 200%, 260%, 50% compared to Stage . The ^{13}C decreased to -27‰ with prominent higher magnitude of variations than that of the previous stages.

3.3 The n-alkanes

The carbon numbers of n-alkanes ranged from C16 to C36. The five stages also showed distinctive proportion of the short-, medium- and long-chain n-alkanes (Figure 3D). Overall, the long-chain n-alkanes dominated among the three classes due to land vegetation effect during the AHP. For example, the long-chain n-alkanes accounted for 59±1% at Stage and increased its proportion to 68±14% at Stage when the 8 peaks were also delineated from significantly higher proportion of long-chain n-alkanes (Figure 3D). Meanwhile, the higher proportion of medium- and short-chain n-alkanes at Stage I (20±0% and 21±1%) than that of Stage (20±7% and 21±8%) (Figure 3D) indicated OC derived from more brackish-water vegetation (higher P_{aq}, Figure 3E) and microorganisms (algae and bacteria) at Stage I (Ficken et al., 2000).

Stage was characterized by the lowest proportion of long-chain n-alkanes (37±18%) but higher proportion of short-chain n-alkanes (46±19%). Similarly, the peaks mentioned in section 3.2 at this stage were also accompanied by the lower proportion of long-chain n-alkanes and the higher proportion of short-chain n-alkanes. The proportion of short-chain n-alkanes decreased (23±16%) at Stage . The P_{aq} values showed a general increasing trend from Stage to (Figure 3E), indicating increased aquatic plant contribution from marine water.

Decreased P_{aq} (Figure 3E) and ^{13}C (Figure 3D) at Stage V suggested more contribution from terrestrial environment. Enhanced long-chain n-alkane input at this stage suggested vegetation input from the Nile catchment.

3.4 GDGTs and their proxies

Different patterns of GDGTs and related BIT index occurred in the five stages of core MZ-1. Stage had increasing abundance of both brGDGTs (54±41 ng/g OC) (Figure 4A) and isoGDGTs (15±16 ng/g OC) (Figure 4B), and decreasing BIT index (0.88±0.14) (Figure 4C) until transiting to Stage , where the three parameters overturned. The concentrations of brGDGTs and isoGDGTs decreased to lower values of 328±278 ng/g OC and 74±92 ng/g OC, while the BIT increased and stabilized at 0.86±0.08.

Stage had increasing abundance of brGDGTs (115±89 ng/g OC, Figure 4A) and isoGDGTs (19±25 ng/g OC, Figure 4B), and decreasing BIT index (0.93±0.05, Figure 4C). Instead, there were decreasing trends in their abundance of brGDGTs (111±84 ng/g OC, Figure 4A) and isoGDGTs (16±19 ng/g OC, Figure 4B) but BIT index (0.94±0.03) increased at the Stage

(Figure 4C). The abundance of brGDGTs (198±148 ng/g OC, Figure 4A) and isoGDGTs (55±56 ng/g OC, Figure 4B) increased at Stage V with lower BIT index (0.84±0.03) (Figure 4C).

The reconstructed pH (precipitation proxy, Figure 4D) and MAAT (temperature proxy, Figure 4E) showed variable trends. The MAAT fluctuated between 15℃ and 20℃, except a few outliers. Stage showed high pH (6.67±0.39, Figure 4D) and low MAAT (17.4±2.8℃, Figure 4E). The pH steadily increased from 6.56±0.07 at Stage to 6.62±0.12 at Stage (Figure 4D), while MAAT at Stage (16.4±0.5℃) subtly declined compared to Stage (17.3±1.3℃) (Figure 4E). An obvious increase in both parameters was observed during Stage , while an increasing pH and abnormal declining temperature appeared in Stage V (Figure 4D, E).

4. Discussion

The well-dated sediment core MZ-1 has shown continuous sedimentary record at decadal-centennial scale (Figures 1, 2). The OC proxies of MZ-1 (Figure 3) showed effective approaches for environmental reconstruction of this study, while reconstructed pH and MAAT enable to reflect hydroclimate fluctuations in the Nile basin, including its delta area (Figure 4). Therefore, the evolution of hydroclimate fluctuations, ecological setting and human activities of the study area can be discussed as below.

4.1 Tetra either lipids: hydroclimate fluctuations

The overall trends of reconstructed pH (Figure 5A) of MZ-1 were similar to the D_{wax} (‰), a sensitive precipitation proxy, recorded in the upstream Tana lake (Costa et al., 2014), Turkana lake (Berke et al., 2012a), Victoria lake (Berke et al., 2012b), and Tanganyika lake (Tierney et al., 2008) (Figure 5B). The overall trends of reconstructed MAAT (Figure 5C) were similar to the temperature record in the Victoria lake (Figure 5D) (Berke et al., 2012b) during ca. 8.0-6.5 ka (Stage I-) (Figure 5D, E), implying that the White Nile was likely the main source of terrigenous OC to the coast (Figure 1A) (Box et al., 2011; Krom et al., 2002; Castañeda et al., 2016). Later on, the decreasing trend of temperature recorded in MZ-1 after ca. 5 ka BP (Figure 5C) was more similar to that of Tana lake (Figure 5E) (Berke et al., 2012), suggesting a potential shift of terrigenous OC sources to the Blue Nile in relation to the southward withdrawing of ITCZ modulated by orbital forcing (Figure 1A) (Box et al., 2011; Hennekam et al., 2015). This had led to the changes in riverine materials to be delivered downstream, and ultimately to influence the ecological setting of the Nile lagoon-coast over time (Box et al., 2011; Castañeda et al., 2016).

The high pH (less precipitation) (Figure 5A) and lower MAAT (Figure 5C) indicated dry and cold climate of the Stage (ca. 8.2-7.7 ka), which depicted the ca. 8.2-ka cold event widely reported in the previous studies (Berger and

Guilaine, 2009; Wanner et al., 2011, Tierney et al., 2017). The abrupt decrease of pH (increased precipitation) and increase of MAAT at the transition between the Stage and (ca. 7.7-5.8 ka) implied the rapid recovery of regional climate from cold-dry to warm-wet conditions. Although the Stage remained generally warm and wet, it gradually cooled (Δ ca. 2-3℃) and dried towards the later stage, indicated by the increasing pH with less precipitation and decreasing MAAT (Figure 5A, C). This implied a gradual aridification of North Africa during the late AHP, due to the southward ITCZ retreatment (Revel et al., 2015). The drying trend was also recorded by decreasing precipitation proxy of D_{wax} (‰) in the upstream lakes (Figure 5B) (Costa et al., 2014; Berke et al., 2012; Tierney et al., 2008). However, a few hydroclimate fluctuations occurred during the AHP (Figure 5A), perhaps due to occasionally abnormal climate feedback to such retreat (Pausata et al., 2020). Episodic enhanced regional precipitation and related Nile flooding thus occurred and likely changed the OC delivery downstream to interact with OC sourced from the marine environment.

The raising pH (Figure 5A) and declining MAAT (Figure 5C) showed that paleoclimate turned to drier and colder during Stage III (ca. 5.8-5.4 ka). In the Stage (ca. 5.4-1.2 ka), however, the MAAT exhibited a rapid increase before declining (Figure 5C), which was comparable to the MAAT record based on brGDGTs reconstruction of Tana lake during this period (Figure 5D, Marsicek et al., 2018; Loomis et al., 2015), demonstrating the long process of climate aridification during the post-AHP. This also met the increasing pH value (less precipitation) during most of stage IV (Figure 5A), and the established climate variabilities in the upstream lakes (Tierney et al., 2008; Berke et al., 2012b; Costa et al., 2014) (Figure 5 D, E). Both MAAT and its variation at Stage V showed different results in the previous studies (Blanchet et al. 2014; Castañeda et al. 2016; Jalali et al., 2017), indicating spatiotemporal heterogeneity of environmental reconstruction in the Anthropocene with human disturbance on the catchment (Martin et al., 2019).

4.2 Bulk OC and n-alkane biomarkers: OC sources and lagoon ecological structure

Established bulk OC and n-alkane biomarkers of MZ-1 can enhance in-depth understanding of OC sources in Holocene, which affected the development of the Nile lagoon ecology.

The Stage has remarkably low bulk OC (Figure 3A) and brGDGTs (Figure 4A), implying less terrestrial OC input, caused by the low Nile sediment discharge during the ca. 8.2-ka cold event. The low C/N (6.7±0.5) and abundant short-chain n-alkanes (Figure 3D) hinted the greater contribution of marine-algae-derived OC (Lamb et al., 2006), in association with strong marine transgression in the Early Holocene (Stanley & Warne, 1993b; Lambeck et al., 2014).

Terrestrial derived OC began to interfere the sedimentary OC pool at the Stage (ca. 7.7-5.8 ka BP) during the AHP. This occurred after the rapid ecological

transition from Stage I to II, characterized by markedly increasing TOC (Figure 3A), long-chain n-alkanes (Figure 3D), and BIT indices (Figure 4C). The Nile flow was rapidly recovered, inferred from the great increase of brGDGTs (Figure 4C) (Hopmans et al., 2004; Fietz et al., 2011). The high pulses (at least 8 times of decadal-centennial scale) of freshwater indicated by the abrupt decrease in ^{13}C and increase in C/N ratio (Figure 3D), together with peaking component of long-chain n-alkanes had played significant role in structuring the coastal ecology (Figure 3D). It appeared that terrestrial OC of the Stage (AHP) had predominantly overrun the marine OC-fed ecology.

Of note, a large amount of terrestrial OC input into the Nile coast during Stage II was also manifested by the widespread deposition of sapropel in the eastern Mediterranean during 7.9-6.5 ka BP (Hennekam et al., 2014; Rohling et al., 2015; van Helmond et al., 2015). The increasing terrestrial OC input was likely from the White Nile as was discussed on the basis of reconstructed MAAT data (seeing 4.1). Additionally, Krom et al (2002) has argued that the sediment flux from the Blue Nile would reduce due to enhanced coverage of vegetation in the Ethiopian Highlands when the Nile flow was higher as a result of northward migration of the ITCZ. Presumably, the primary production in the Nile lagoon was thus catalyzed by sufficient dissolved phosphate caused by less removal by particulates (Krom et al., 2002).

The Manzala lagoon-coast changed to a more brackish-water eco-setting at Stage (5.8-5.4 ka), the end of AHP (Bernhardt et al., 2012). Obviously, terrestrial OC reduced as was indicated from the decrease of long-chain n-alkanes (Figure 3D). The Nile flow reduced significantly in response to the mega-drying condition (Weldeab et al., 2014; Revel et al., 2015). In fact, several droughts can be inferred from the lows of C/N and depleted ^{13}C isotopes (Figure 3D). The increased macrophytes (high P_{aq}, Figure 3E) and local microorganisms (high proportion of medium- and short-chain n-alkanes) (Figure 3D) at this stage resulted in aquatic vegetation (macrophytes), implying more brackish water in nature.

Comparing the Stage , the short-chain n-alkanes of marine origin decreased and the long-chain n-alkanes of terrestrial origin increased in Stage , reflecting shrunken Nile water and sediment into lagoon-coast since ca. 5.4 ka BP. This was also seen from the remarkably decreasing sedimentation rate (ca. 0.03 cm/year) after ca. 5 ka (Figure 2C). In addition, the Stage V was characterized by the abrupt pulses in almost all proxies (Figure 3), hinting strong influences from intensifying human activities (discussed below).

The biplot of ^{13}C vs. C/N signified the transformation of sedimentary OC sources from marine (Stage I) to terrestrial soil and brackish macrophytes at Stages - , and to human intervened terrestrial OC input at Stages -V (Figure 6A; Lamb et al., 2006). PCA biplot separated the parameters into a few clusters (Figure 6B), confirming different extent from aquatic vs. terrestrial vs. anthropogenic effects on ecological development among the five stages. Quantitatively, 62.7±4.6% was contributed from the marine algae at Stage I, and the

proportion reduced to 24.5±2.2% at Stage , with an average of 130% increase of terrestrially-derived OC during the immense Nile flooding of the AHP (Figure 6C, Table 2). Stage was featured with 77% increase of OC from macrophytes since Stage I (19.9±3.3%), the highest macrophytes (35.3±3.1%) contribution when the early-Holocene marine transgression occurred. The macrophytes OC increased to 36.7±11.6% at Stage but reduced to 32.2±7.5% at Stage V. Correspondingly, the soil contribution increased by 7% (Figure 6C, Table 2) mostly due to human interfered land erosion.

4.3 Biogeochemical and charcoal proxies: Early human activities

There is a long history of the early human activities in the Nile Delta, which can be traced back to at least 6000 years ago (Buzter, 1976; Hawass et al., 1988). The recent study by Zhao et al. (2020) has revealed that the early farming at the archaeological site of Sais (Haggar) of the central-west Nile Delta was as of ca 7000 years ago. Similarly, the early human occupation in the well-known Samara area (ca. 40 km upstream of the MZ-1 site, Figure 1B) of central-east Nile Delta also started at least 6000 years ago (Tristant & De Dapper, 2009).

Abnormal pulses of terrestrial TOC, TN and ^{13}C in the Stage IV (Figure 3A-C) were intuitively thought to be derived from land modification by the early settlers who were engaged in herding and farming in Samara area (Tristant & De Dapper, 2009). These OC proxies became even higher at the Stage V (Figure 3A-C), corroborating intensification of land exploitation in the recent millennia. Undoubtedly, land reclamation against the long-aridification after the AHP raised enormous terrestrial OC input into downstream lagoon coast, transported via old Nile branches existed in the study area during the early-middle Holocene (Buzter, 1976). Besides, the prominent increase in ^{15}N to +6‰ during Stage V (Figure 3C) reflected the presence of animal and/or sewage waste due to human activities (Heaton, 1986), because ^{15}N is lower in phytoplankton and terrestrial vegetation (about 1-3‰) (Douglas et al., 2004). As result, nutrient enrichment enhanced growth of lagoon algae and eutrophication (Dubois et al., 2018), which was in turn to increase the TOC and TN in lagoon eco-setting (Figure 3A, B).

To testify human impact on lagoon ecology, we used charcoal flux of MZ-1 to further argue with the modification on coastal landscape. The relatively stable distribution of charcoal flux (both micro- and macro-) and the L/W ratio before ca. 6 ka (ca. 10 m below) hints lowly modified landscape in the study area (Figure 2D). However, the highly fluctuated charcoal fluxes since then enabled to link to the intensification of human activities in the upstream Samara settlement area. The charcoal fluxes, especially the macro-charcoal (>100 um) has been used as the most effective indicator for tracing land reclamation through clearing-firing processes at/near archaeological site in the early human farming history (Zong et al., 2007). Although charcoals of MZ-1 were not primary due to re-transportation, the high-frequency of temporal fluctuations with long-term

(millennial) scale since ca. 6 ka would shed lights on the early land reclamation in the Nile Delta, and related OC input to the lagoon ecological development.

5. Conclusions

The multi-proxy analyses of OC and biomarkers in sediment core MZ-1 of the Nile coast witnessed the distinctive processes and related mechanism for the significant changes in hydroclimate, ecological setting and human activities during the Holocene. Marine transgression and low Nile discharge occurred at ca. 8.2-7.7 ka (Stage I), leading to the high proportion of marine OC for building the lagoon ecology. The 8.2-ka cold event was identified by the low MAAT and high pH proxies (less precipitation). Terrestrial OC played its increasing role in nourishing lagoon eco-setting in context of numerous freshwater pulses during the AHP (Stage ; ca. 7.7-5.8 ka). Peaks of C/N, ^{13}C and long-chain n-alkanes values signified episodic immense Nile floods at decadal-centennial scales. The increasing pH and decreasing MAAT based on tetra either lipids suggested the Holocene hydroclimatic changes from warm-wet condition at Stage , to cold-dry condition at Stage , accompanied with increased brackish macrophytes deposition enhanced medium-chain n-alkanes contribution. The human disturbance on natural environments may have started as of ca. 6 ka (Stage) through land exploitation by the early human occupation, evidenced by both abnormally pulsed OC and charcoal fluxes. The overwhelming human OC did not emerge until the last millennium (Stage V), seen by the abrupt variations in almost all OC proxies and charcoal data. Overall, this study enhances in-depth understanding of the interactions among hydroclimate, land-ocean interactions and early human activities on building the lagoon ecology of the Nile Delta.

Acknowledgements

We thank Bingyan Zhao, Zhaoyang Sun, and Zuhong Hu for laboratory support at GIGCAS. This work was supported by the China Postdoctoral Science Foundation funded project (2020M671878), State Key Laboratory of Organic Geochemistry, GIGCAS (SKLOG202021), National Science Foundation of China (41620104004, 42076029, 91851210), and the Open Research Fund of State Key Laboratory of Estuarine and Coastal Research (SKLEC-KF202005), and Shenzhen Key Laboratory of Marine Archaea Geo-Omics, Southern University of Science and Technology (ZDSYS20180208184349083), Shenzhen International Cooperation Research Project (GJHZ20180928155004783).

Data availability

The datasets used in this study could be accessible through Figshare (https://figshare.com/s/e731dbb039b0fad5ed48).

Reference

Abebe, G., Tsunekawa, A., Haregeweyn, N., Takeshi, T., Wondie, M., Adgo, E., Masunaga, T., Tsubo, M., Ebabu, K., Berihun, M.L., Tassew, A. (2020). Effects of Land Use and Topographic Position on Soil Organic Carbon and Total Nitrogen Stocks in Different Agro-Ecosystems of the Upper Blue Nile Basin. Sustainability, 12(6), 2425.

Awiti, A.O., Walsh, M.G., Kinyamario, J. (2008). Dynamics of topsoil carbon and nitrogen along a tropical forestecropland chronosequence: evidence from stable isotope analysis and spectroscopy. Agriculture, Ecosystems & Environment, 127, 265-272.

Berger, J.-F., & Guilaine, J. (2009). The 8200 cal BP abrupt environmental change and the Neolithic transition: A Mediterranean perspective. Quaternary International, 200(1), 31–49.

Berke, M. A., Johnson, T. C., Werne, J. P., Schouten, S., Damsté, J. S. S. (2012a). A mid-Holocene thermal maximum at the end of the African Humid Period. Earth and Planetary Science Letters, 351, 95–104.

Berke, M.A., Johnson, T.C., Werne, J.P., Grice, K., Schouten, S., Sinninghe Damsté, J.S. (2012b). Molecular records of climate variability and vegetation response since the Late Pleistocene in the Lake Victoria basin, East Africa. Quaternary Science Reviews, 55, 59–74.

Bernhardt, C. E., Horton, B. P., Stanley, J.-D. (2012). Nile Delta vegetation response to Holocene climate variability. Geology, 40(7), 615–618.

Blaauw, M., & Christen, J. A. (2011). Flexible paleoclimate age-depth models using an autoregressive gamma process. Bayesian Analysis, 6(3), 457–474.

Blanchet, C. L., Frank, M., Schouten, S. (2014). Asynchronous Changes in Vegetation, Runoff and Erosion in the Nile River Watershed during the Holocene. PLOS ONE, 9(12).

Box, M. R., Krom, M. D., Cliff, R. A., Bar-Matthews, M., Almogi-Labin, A., Ayalon, A., Paterne, M. (2011). Response of the Nile and its catchment to millennial-scale climatic change since the LGM from Sr isotopes and major elements of East Mediterranean sediments. Quaternary Science Reviews, 30(3), 431–442.

Bush, R. T., & McInerney, F. A. (2013). Leaf wax n-alkane distributions in and across modern plants: Implications for paleoecology and chemotaxonomy. Geochimica et Cosmochimica Acta, 117, 161–179.

Butzer, K. W. (1976). Early hydraulic civilization in Egypt: A study in cultural ecology. Chicago: University of Chicago Press, 134p.

Castañeda, I. S., Schouten, S., Pätzold, J., Lucassen, F., Kasemann, S. A., Kuhlmann, H., Schefuß, E. (2016). Hydroclimate variability in the Nile River

Basin during the past 28,000 years. Earth and Planetary Science Letters, 438, 47–56.

Chandan, D., & Peltier, W. R. (2020). African Humid Period precipitation sustained by robust vegetation, soil, and lake feedbacks. Geophysical Research Letters, 47(21).

Clarke, J., Brooks, N., Banning, E.B., Bar-Matthews, M., Campbell, S., Clare, L., Cremaschi, M., di Lernia, S., Drake, N., Gallinaro, M., Manning, S., Nicoll, K., Philipm, G., Rosen, S., Schoop, U.-D., Tafuri, M.A., Weninger, B., Zerbonig, A. (2016). Climatic changes and social transformations in the Near East and North Africa during the 'long' 4th millennium BC: a comparative study of environmental and archaeological evidence. Quaternary Science Reviews, 136, 96-121.

Costa, K. M., Russell, J., Konecky, B., Lamb, H. (2014). Isotopic reconstruction of the African Humid Period and Congo Air Boundary migration at Lake Tana, Ethiopia. Quaternary Science Reviews, 83, 58–67.

De Jonge, C., Hopmans, E. C., Zell, C. I., Kim, J. H., Schouten, S., Damsté, J. S. S. (2014). Occurrence and abundance of 6-methyl branched glycerol dialkyl glycerol tetraethers in soils: Implications for palaeoclimate reconstruction. Geochimica et Cosmochimica Acta, 141, 97–112.

deMenocal, P., Ortiz, J. D., Guilderson, T., Adkins, J., Sarnthein, M., Baker, L., Yarusinsky, M. (2000). Abrupt onset and termination of the African Humid Period: rapid climate responses to gradual insolation forcing. Quaternary Science Reviews, 19(1), 347–361.

Douglas, M. S. V., Smol, J. P., Savelle, J. M., Blais, J. M. (2004). Prehistoric Inuit whalers affected Arctic freshwater ecosystems. Proceedings of the National Academy of Sciences of the United States of America, 101(6), 1613–1617.

Dubois, N., Saulnier-Talbot, E., Mills, K., Gell, P., Battarbee, R., Bennion, H., Chawchai, S., Dong, X.H., Francus, P., Flower, R., Gomes, D.F., Gregory-Eavers, I., Humane, S., Kattel, G., Jenny, J.P., Langdon, P., Massaferro, J., McGowan, S., Mikomagi, A., Ngoc, N.M., Ratnayake, A.S., Reid, M., Rose, N., Saros, J., Schillereff, D., Tolotti, M., Valero-Garces, B. (2018). First human impacts and responses of aquatic systems: A review of palaeolimnological records from around the world. The Anthropocene Review, 5(1), 28–68.

Ficken, K., Li, B., Swain, D., Eglinton, G. (2000). An n-alkane proxy for the sedimentary input of submerged/floating freshwater aquatic macrophytes. Organic Geochemistry, 31(7), 745–749.

Fietz, S., Martínez-Garcia, A., Huguet, C., Rueda, G., Rosell-Melé, A. (2011). Constraints in the application of the Branched and Isoprenoid Tetraether index as a terrestrial input proxy. Journal of Geophysical Research, 116(C10032).

Fry, B., Sherr, E.B. (1989). Δ13C measurements as indicators of carbon flow in marine and freshwater ecosystems. P.W. Rundel, J.R. Ehleringer, K.A. Nagy

(Eds.), Stable Isotopes in Ecological Research, Springer, New York, pp. 196-229.

Garcin, Y., Melnick, D., Strecker, M. R., Olago, D., Tiercelin, J.-J. (2012). East African mid-Holocene wet–dry transition recorded in palaeo-shorelines of Lake Turkana, northern Kenya Rift. Earth and Planetary Science Letters, 331, 322–334.

Gasse, F. (2000). Hydrological changes in the African tropics since the Last Glacial Maximum. Quaternary Science Reviews, 19(1), 189–211.

Hawass, Z., Hassan. F.A., and Gautier, A. (1988). Chronology, Sediments, and Subsistence at Merimda Beni Salama. The Journal of Egyptian Archaeology, 74, 31–38.

Heaton, T. H. (1986). Isotopic studies of nitrogen pollution in the hydrosphere and atmosphere: A review. Chemical Geology: Isotope Geoscience Section, 59(1), 87–102.

Heaton, T. J., Köhler, P., Butzin, M., Bard, E., Reimer, R. W., Austin, W. E. N., Bronk Ramsey, C., Grootes, P. M., Hughen, K. A., Kromer, B., Reimer, P. J., Adkins, J., Burke, A., Cook, M. S., Olsen, J., Skinner, L. C. (2020). Marine20—The Marine Radiocarbon Age Calibration Curve (0–55,000 cal BP). Radiocarbon, 62(4), 779–820.

Hedges, J. I. & Oades, J. M. (1997). Comparative organic geochemistries of soils and sediments, Organic Geochemistry, 27, 319–361.

Hennekam, R., Jilbert, T., Schnetger, B., Lange, G. J. de. (2014). Solar forcing of Nile discharge and sapropel S1 formation in the early to middle Holocene eastern Mediterranean. Paleoceanography, 29(5), 343–356.

Hopmans, E.C., Weijers, J.W.H., Schefuss, E., Herfort, L., Sinninghe Damsté, J.S., Schouten, S. (2004). A novel proxy for terrestrial organic matter in sediments based on branched and isoprenoid tetraether lipids. Earth and Planetary Science Letters, 24, 107–116.

Jalali, B., Sicre, M.-A., Kallel, N., Azuara, J., Combourieu-Nebout, N., Bassetti, M.-A., Klein, V. (2017). High-resolution Holocene climate and hydrological variability from two major Mediterranean deltas (Nile and Rhone). The Holocene, 27(8), 1158–1168.

Johnson, D. W., Hanson, P. J., Todd, D. E., Susfalk, R. B., Trettin, C. C. (1998). Precipitation Change and Soil Leaching: Field Results and Simulations from Walker Branch Watershed, Tennessee. Water Air and Soil Pollution, 105(1), 251–262.

Khedr, A. H. A., & El-Demerdash, M. A. (1997). Distribution of aquatic plants in relation to environmental factors in the Nile Delta. Aquatic Botany, 56(1), 75–86.

Krom, M. D., Stanley, U. J. D., Cliff, R. A., Woodward, J. C. (2002). Nile River sediment fluctuations over the past 7000 yr and their key role in sapropel

development. Geology, 30(1), 71–74.

Kuper, R., & Kroepelin, S. (2006). Climate-controlled Holocene occupation in the Sahara: Motor of Africa's evolution. Science, 313(5788), 803–807.

Lamb, A. L., Wilson, G. P., Leng, M. J. (2006). A review of coastal palaeoclimate and relative sea-level reconstructions using 13C and C/N ratios in organic material. Earth-Science Reviews, 75(1), 29–57.

Lambeck, K., Rouby, H., Purcell, A., Sun, Y., Sambridge, M. (2014). Sea level and global ice volumes from the Last Glacial Maximum to the Holocene. Proceedings of the National Academy of Sciences of the United States of America, 111(43), 15296–15303.

Li, X., Bianchi, T. S., Yang, Z., Osterman, L. E., Allison, M. A., DiMarco, S. F., Yang, G. (2011). Historical trends of hypoxia in Changjiang River estuary: Applications of chemical biomarkers and microfossils. Journal of Marine Systems, 86(3-4), 57-68.

Li, X., Bianchi, T. S., Allison, M. A., Chapman, P., Yang, G. (2013). Historical reconstruction of organic carbon decay and preservation in sediments on the East China Sea shelf, Journal of Geophysical Research: Biogeosciences, 118(3), 1079–1093.

Loomis, S. E., Russell, J. M., Lamb, H. F. (2015). Northeast African temperature variability since the Late Pleistocene. Palaeogeography, Palaeoclimatology, Palaeoecology, 423, 80–90.

Marshall, M. H., Lamb, H. F., Huws, D., Davies, S. J., Bates, R. J., Bloemendal, J., Boyle, J., Leng, M.J., Umer, M., Bryant, C. (2011). Late Pleistocene and Holocene drought events at Lake Tana, the source of the Blue Nile. Global and Planetary Change, 78(3), 147–161.

Marsicek, J., Shuman, B. N., Bartlein, P. J., Shafer, S. L., Brewer, S. (2018). Reconciling divergent trends and millennial variations in Holocene temperatures. Nature, 554(7690), 92–96.

Martin, C., Menot, G., Thouveny, N., Davtian, N., Andrieu-Ponel, V., Reille, M., Bard, E. (2019). Impact of human activities and vegetation changes on the tetraether sources in Lake St Front (Massif Central, France). Organic Geochemistry, 135, 38-52.

Meyers, P. A. (1994). Preservation of elemental and isotopic source identification of sedimentary organic matter. Chemical Geology, 114, 289–302.

Pausata, F. S. R., Gaetani, M., Messori, G., Berg, A., de Souza., D. M., Sage, R. F., deMenocal, P. B. (2020). The greening of the sahara: Past changes and future implications. One Earth, 2(3), 235– 250.

Pennington, B., Sturt, F., Wilson, P., Rowland, J., Brown, A. (2017). The fluvial evolution of the Holocene Nile Delta. Quaternary Science Reviews, 170, 212–231.

Rachmayani, R., Prange, M. Schulz, M. (2015). North African vegetation–precipitation feedback in early and mid-Holocene climate simulations with CCSM3-DGVM. Climate of Past, 11, 175–185.

Reimer, P. J., Austin, W. E. N., Bard, E., Bayliss, A., Blackwell, P. G., Bronk Ramsey, C., Cheng, H., Edwards, R. L., Friedrich, M., Grootes, P. M., Guilderson, T. P., Hajdas, I., Heaton, T. J., Hogg, A. G., Hughen, K. A., Kromer, B., Manning, S. W., Muscheler, R., Palmer, J. G., Pearson, C., van der Plicht, J., Reimer, R. W., Richards, D. A., Scott, E. M., Southon, J. R., Turney, C. S. M., Wacker, L., Adolphi, F., Büntgen, U., Capano, M., Fahrni, S. M., Fogtmann-Schulz, A., Friedrick, R., Köhler, P., Kudsk, S., Miyake, F., Olsen, J., Reinig, F., Sakamoto, M., Sookdeo, A., Talamo, S. (2020). The IntCal20 Northern Hemisphere Radiocarbon Age Calibration Curve (0–55 cal ka BP). Radiocarbon, 62(4), 725–757.

Revel, M., Ducassou, E., Skonieczny, C., Colin, C., Bastian, L., Bosch, D., Migeon, S., Mascle, J. (2015). 20,000 years of Nile River dynamics and environmental changes in the Nile catchment area as inferred from Nile upper continental slope sediments. Quaternary Science Reviews, 130, 200–221.

Rohling, E.J., Marino, G., Grant, K.M. (2015). Mediterranean climate and oceanography, and the periodic development of anoxic events (sapropels). Earth-Science Review, 143, 62-97.

Said, R. (1993). The river Nile, Geology, Hydrology and Utilization. Oxford: Pergamon Press, 320p.

Schouten, S., Hopmans, E. C., Damsté, J. S. S. (2013). The organic geochemistry of glycerol dialkyl glycerol tetraether lipids: A review. Organic Geochemistry, 54, 19–61.

Shanahan, T. M., Mckay, N. P., Hughen, K. A., Overpeck, J. T., Otto-Bliesner, B., Heil, C. W., King, J., Scholz, C.A., Peck, J. (2015). The time-transgressive termination of the African Humid Period. Nature Geoscience, 8(2), 140–144.

Sheashaa H., Zhao, X.S., Salem A., Liu, Y., Lai, X.H., Chen, Z.Y. (2018). Early-middle Holocene climatic and environmental changes in the Nile delta and implications for early agriculture. Journal of Lake Sciences, 30(3):857-864.

Stanley, D. J., & Warne, A. G. (1993a). Sea level and initiation of Predynastic culture in the Nile delta. Nature, 363(6428), 435–438.

Stanley, D. J., & Warne, A. G. (1993b). Nile Delta: Recent geological evolution and human impact. Science, 260(5108), 628–634.

Tierney, J. E., Russell, J. M., Huang, Y., Damsté, J. S. S., Hopmans, E. C., Cohen, A. S. (2008). Northern Hemisphere Controls on Tropical Southeast African Climate During the Past 60,000 Years. Science, 322(5899), 252–255.

Tierney, J. E., Pausata, F. S. R., deMenocal, P. B. (2017). Rainfall regimes of the green Sahara. Science Advances, 3(1), e1601503.

Tristant, Y., & De Dapper, M. (2009). Predynastic man and landscape in the Samara area. Ol' Man River: geo-archaeological aspects of rivers and river plains. In Archaeological Reports Ghent University 5. p.601-617.

van Helmond, N. A. G. M., Hennekam, R., Donders, T. H., Bunnik, F. P. M., Lange, G. J. de, Brinkhuis, H., Sangiorgi, F. (2015). Marine productivity leads organic matter preservation in sapropel S1: palynological evidence from a core east of the Nile River outflow. Quaternary Science Reviews, 108, 130–138.

Wanner, H., Solomina, O., Grosjean, M., Ritz, S. P., Jetel, M. (2011). Structure and origin of Holocene cold events. Quaternary Science Reviews, 30(21), 3109–3123.

Weijers, J. W. H., Schouten, S., van den Donker, J. C., Hopmans, E. C. Sinninghe Damsté, J. S. (2007). Environmental controls on bacterial tetraether membrane lipid distribution in soils. Geochimica et Cosmochimica Acta, 71, 703–713.

Weldeab, S., Menke, V., Schmiedl, G. (2014). The pace of East African monsoon evolution during the Holocene. Geophysical Research Letters, 41(5), 1724–1732.

Woodward, J. C., Macklin, M. G., Krom, M. D., Williams, M. A. J. (2007). The Nile: Evolution, Quaternary River Environments and Material Fluxes. In: A. Gupta, Editor(s). Large Rivers: Geomorphology and Management. Chichester: John Wiley & Sons, p. 261-292.

Xiao, W., Wang, Y., Zhou, S., Hu, L., Yang, H., Xu, Y. (2016). Ubiquitous production of branched glycerol dialkyl glycerol tetraethers (brGDGTs) in global marine environments: a new source indicator for brGDGTs. Biogeosciences, 13, 5883-5894.

Zhao, X.S, Thomas, I., Salem, A., Alassal, S. E., Liu, Y., Sun, Q.L., Chen, J., Ma, F.W., Finlayson, B., Chen, Z.Y. (2020). Holocene climate change and its influence on early agriculture in the Nile Delta, Egypt. Palaeogeography, Palaeoclimatology, Palaeoecology, 547, 109702.

Zong, Y.Q., Chen, Z., Innes, J.B., Chen, C., Wang, Z., and Wang, H. (2007), Fire and flood management of coastal swamp enabled first rice paddy cultivation in east China. Nature, 449, 459-462.

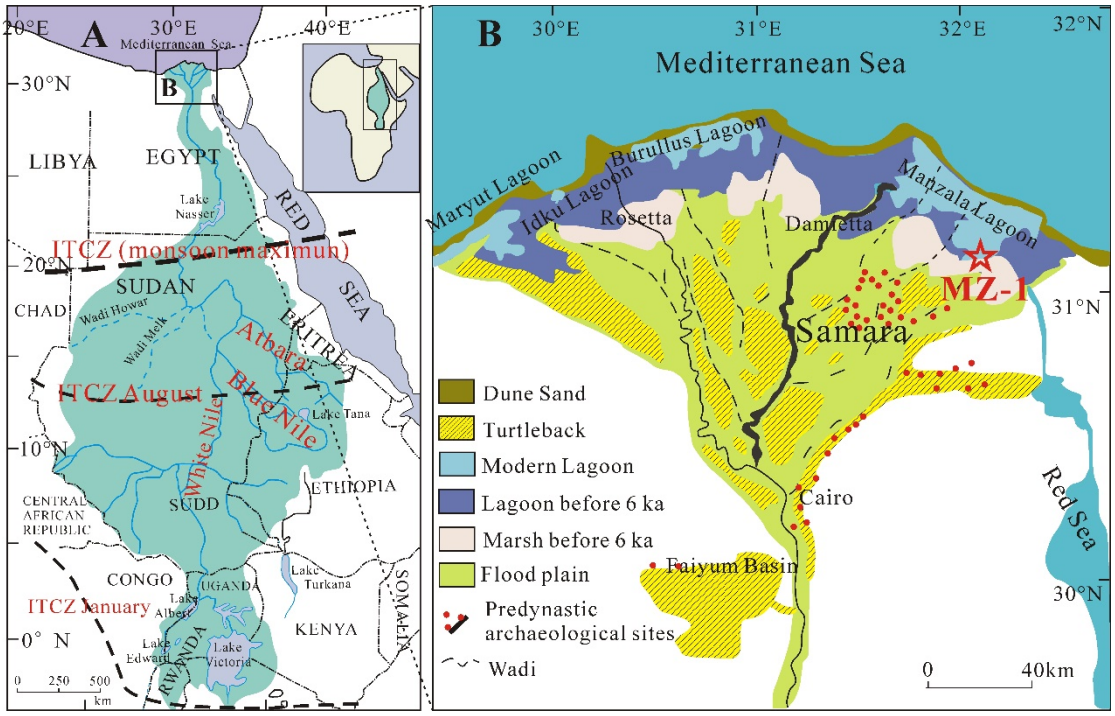
A
20°E
30°E
40°E
Mediterranean Sea
B
30°N
LIBYA
EGYPT
Lake Nasser
RED SEA
ITCZ (monsoon maximun)
20°N
SUDAN
CHAD
Wadi Howar
Wadi Melk
ERITREA
Atbara
Blue Nile
ITCZ August
Lake Tana
White Nile
10°N
ETHIOPIA
SUDD
CENTRAL AFRICAN REPUBLIC
CONGO
UGANDA
Lake Albert
Lake Turkana
SOMALIA
ITCZ January
KENYA
0° N
Lake Edward
Lake Victoria
RWANDA
0 250 500 km
B
30°E
31°E
32°E
32°N
Mediterranean Sea
Maryut Lagoon
Burullus Lagoon
Idku Lagoon
Rosetta
Damietta
Manzala Lagoon
MZ-1
31°N
Samara
Dune Sand
Turtleback
Modern Lagoon
Lagoon before 6 ka
Marsh before 6 ka
Flood plain
Predynastic archaeological sites
Wadi
Cairo
Red Sea
Faiyum Basin
30°N
0 40km

Figure 1 A) The Nile drainage basin (modified after Woodward et al., 2007). The White Nile, the Blue Nile, and the Atbara branches are labelled. Black dashed line denotes the approximate position of ITCZ at present August and the Holocene monsoon maximum (Gasse, 2000); B) The Nile Delta and the study site of Core MZ-1 at Manzala Lagoon (modified from Butzer, 1976).

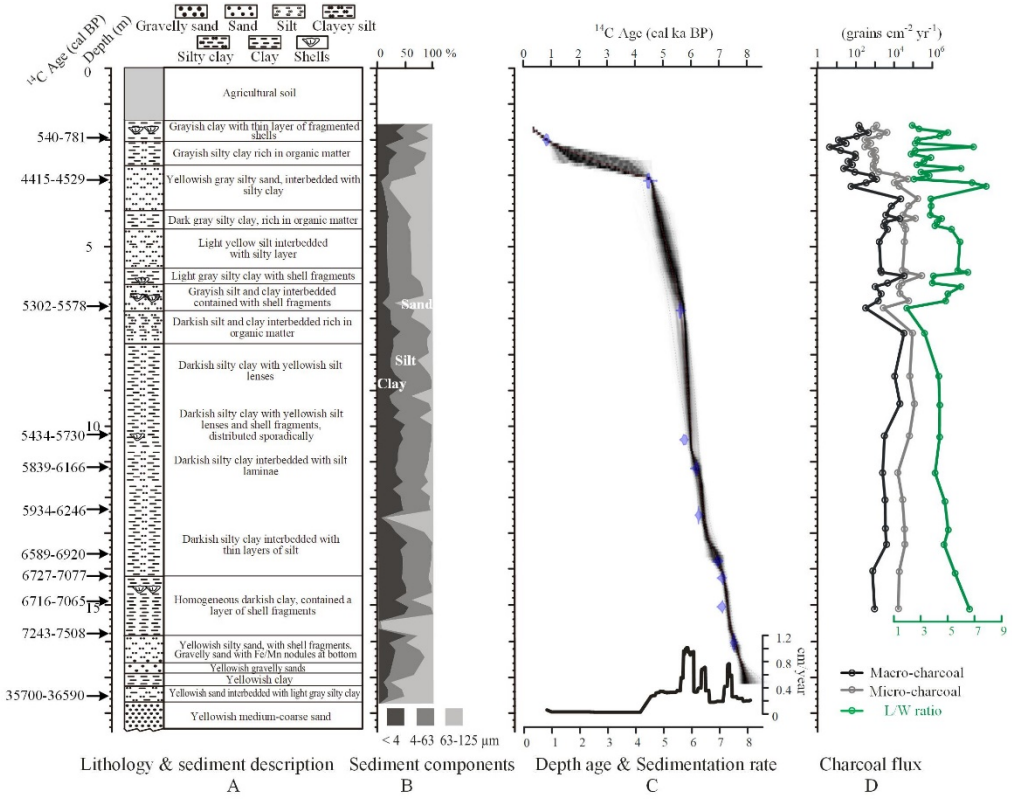

Figure 2 A) Well-^{14}C-dated sediment core MZ-1; B) Sediment components; C) Bayesian-modeled age-depth curve and sedimentation rate of the core; D) Micro-and macro-charcoal fluxes, and median length/width (L/W) ratio.

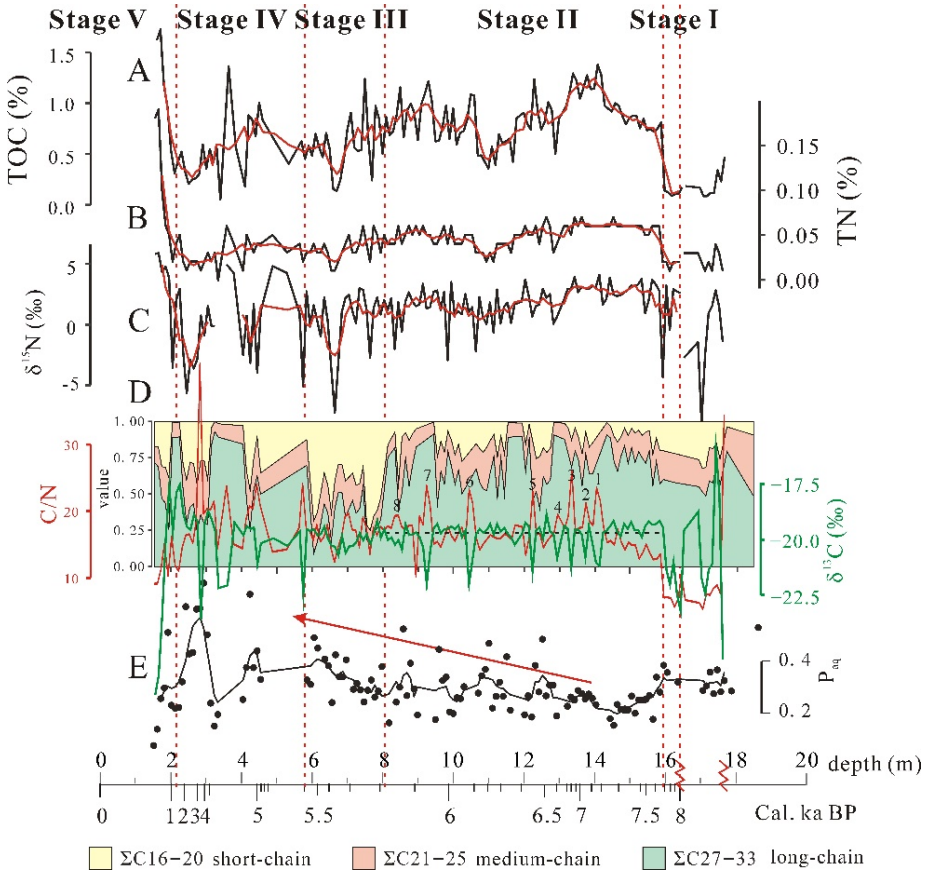

Figure 3 The bulk carbon and n-alkane results of core MZ-1. A) TOC; B) TN; C) ^{15}N; D) ^{13}C, C/N, and proportions of n-alkanes; E) P_{aq} proxy. The red curves in A, B and C, the red (C/N) and green (^{13}C) curves in D and the black curve in E, were five-point smoothed data. The numbered highs in D denoting 8 oscillations of terrestrial vs. marine OC at decadal-centennial scale during the AHP.

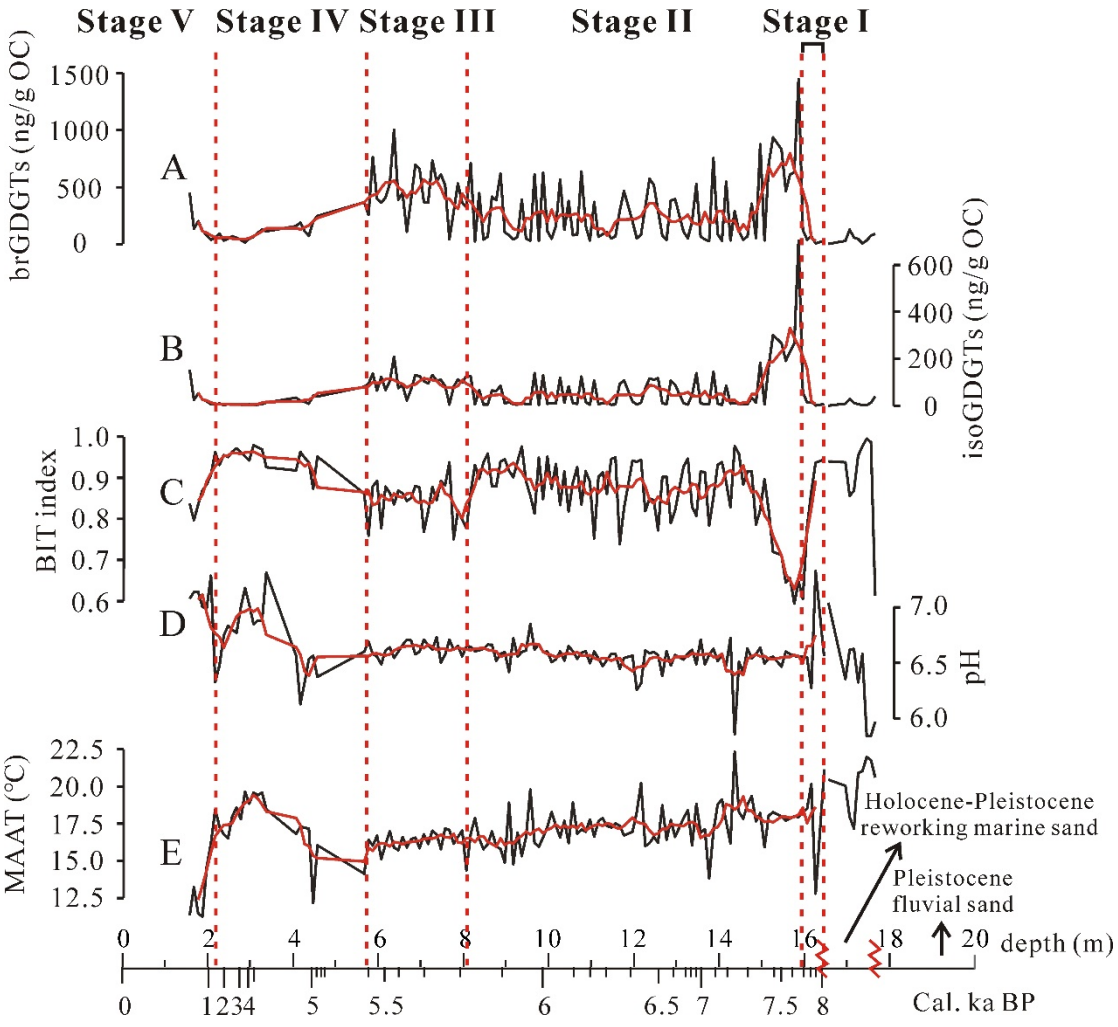

Figure 4 GDGTs and proxies of core MZ-1. A) BrGDGTs concentrations; B) IsoGDGTs concentrations; C) BIT index; D) soil pH; E) MAAT (Mean annual air temperature). The red line in each figure denotes 5-point smoothing values.

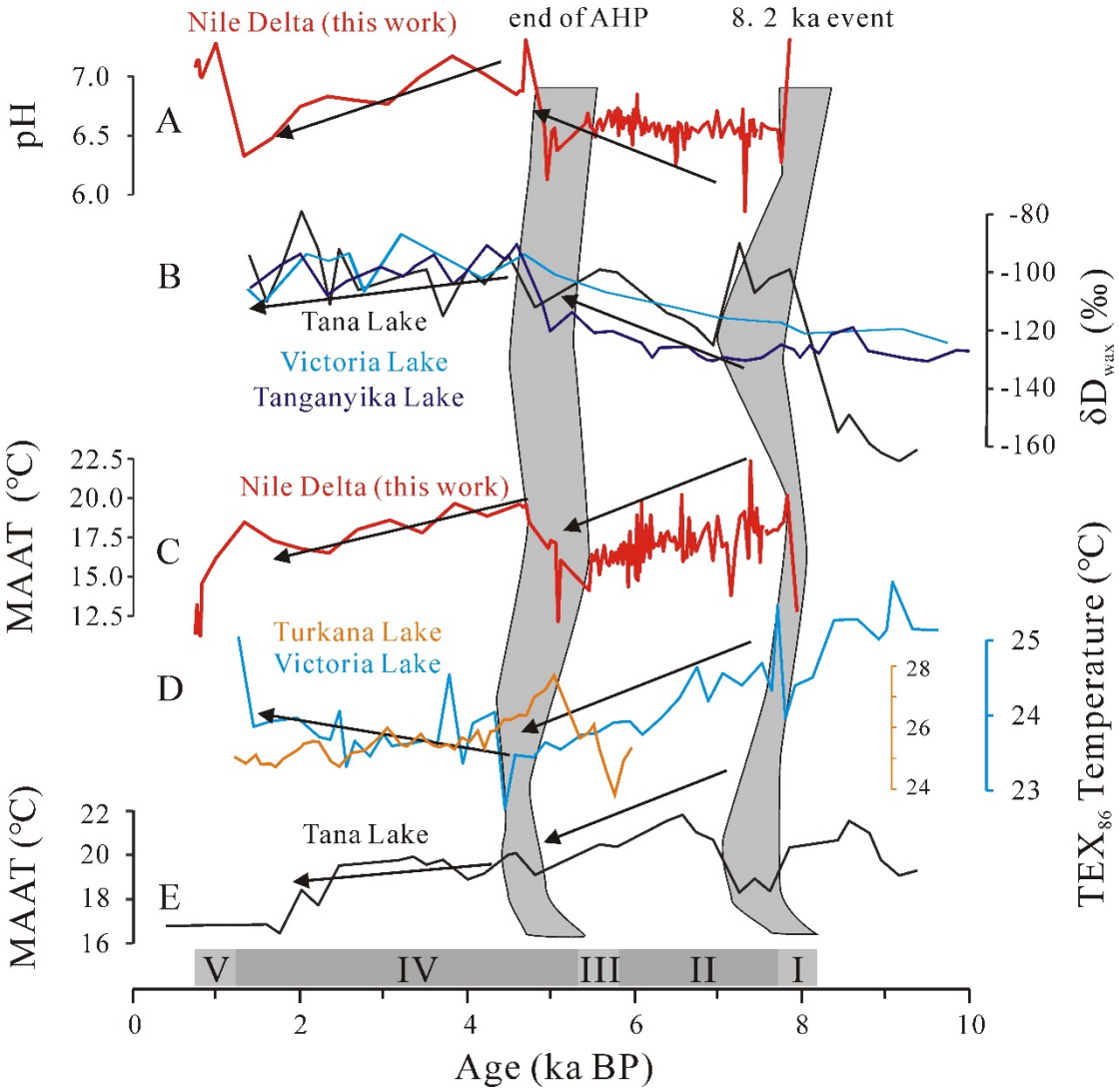

Figure 5 The multi-proxies of hydroclimatic changes during the Holocene. A) Reconstructed pH of the Nile Delta (this study); B) D_{wax} (‰) (precipitation proxy) of Tana lake (Costa et al., 2014), Victoria lake (Berke et al., 2012b), and Tanganyika lake (Tierney et al., 2008); C) TEX_{86} calibrated temperature of Turkana lake and Victoria lake (Berke et al., 2012a, b); D) MAAT reconstruction of the Nile Delta (this work); E) MAAT reconstruction of Tana lake (Loomis et al., 2015).

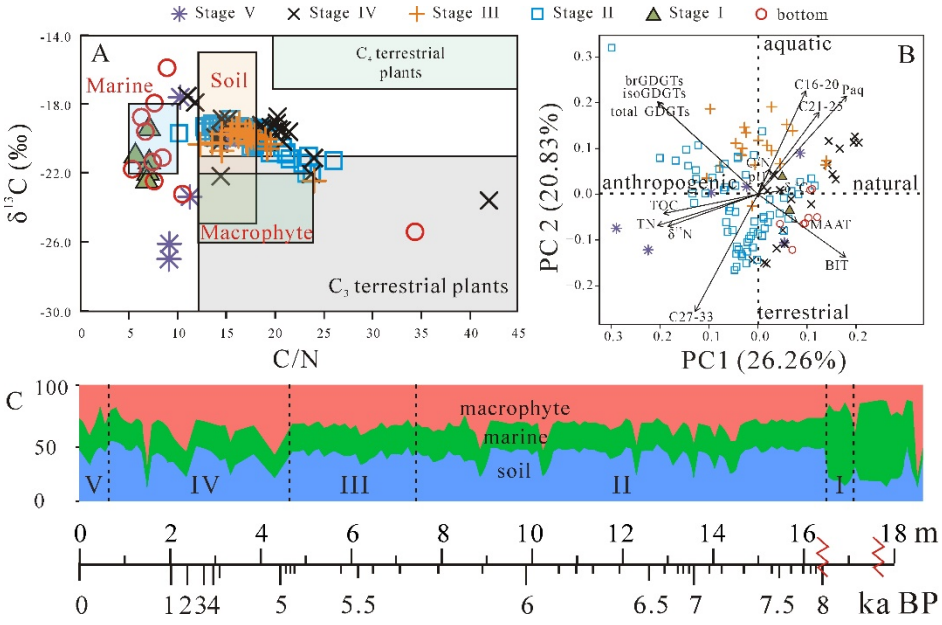

Figure 6 A) Cross plots of C/N ratios against ^{13}C of Core MZ-1. B) Principal Component Analysis (PCA) showing the multivariate variation of all samples and main proxies. C) Three end-member (marine algae, terrestrial soil, and macrophytes) modeling of the organic carbon.

Table 1 Details of AMS ^{14}C dating materials of MZ-1 core

Depth (m)	Conventional Radiocarbon Age (yr BP)	Calibrated Age (2) (cal. yr BP)	Materials
	±30	-781	shell
	±30	-4529	charcoal
	±30	-5578	shell
	±30	-5730	shell
	±30	-6166	shell
	±30	-6246	shell
	±30	-6920	shell
	±30	-7077	shell
	±30	-7065	shell
	±30	-7508	shell
	±190	-36590	charcoal

Table 2 Endmember mixing model results

	Soil	Marine	Macrophyte			
%	Mean	SE	Mean	SE	Mean	SE
Stage V	40.8	5.2	27.0	3.7	32.2	7.5
Stage	38.1	10.3	25.2	3.3	36.7	11.6
Stage	40.3	3.6	24.4	1.2	35.3	3.1
Stage	40.5	6.9	24.5	2.2	35.0	6.2
Stage I	17.5	2.3	62.7	4.6	19.9	3.3